Precipitation variability related to atmospheric circulation patterns over the Tibetan Plateau

(article starts on next page)

RESEARCH ARTICLE

Precipitation variability related to atmospheric circulation patterns over the Tibetan Plateau

Hui-Wen Lai[1] | Deliang Chen[1] | Hans W. Chen[2]

[1]Department of Earth Sciences, University of Gothenburg, Gothenburg, Sweden

[2]Department of Space, Earth and Environment, Chalmers University of Technology, Gothenburg, Sweden

Correspondence
Deliang Chen, Department of Earth Sciences, University of Gothenburg, Gothenburg, Sweden.
Email: deliang@gvc.gu.se

Abstract

Precipitation is affected by intricate atmospheric dynamic and thermodynamic processes. Horizontal winds are frequently used to represent the dynamic component as winds play a critical role in transporting moisture. Previous studies on precipitation over the Tibetan Plateau (TP) focused on the influence of summer monsoons and westerlies in isolation. However, the collective seasonal dynamics and their combined effects on the precipitation distribution remain less explored. This study aims to determine the seasonal evolutions of the wind patterns and the associated regional precipitation patterns over the TP using a neural network approach and focuses on their interannual variability and long-term trends. A self-organizing map (SOM) was used to classify the wind patterns based on 500 hPa winds and related precipitation from the ERA5 reanalysis. The classified wind patterns show seasonal shifts between the Asian summer monsoon circulations and the westerlies along with the westerly jets migrating between the north and south of the TP from summer to winter. The locations of abundant precipitation during the winter and transition seasons are mainly associated with variations in the intensity and locations of the strong westerlies. There is a significant positive trend in the occurrences of the summer-type wind pattern, which has likely led to a wetter TP, and an earlier-ended winter and advanced spring wind patterns. The interannual variability of westerlies is highly related to the variability of precipitation in the western TP during its wet season (January–April). In the eastern TP, the interannual variability of the precipitation is linked to the wind patterns associated with the westerly jets to the south of the TP, while precipitation variability in the central TP is controlled by thermodynamic components. This study reveals the spatial precipitation distributions according to the different wind patterns and identifies the contributions from atmospheric components to the regional precipitation over the TP.

KEYWORDS
monsoons, precipitation, self-organizing map, Tibetan Plateau, westerlies

1 | INTRODUCTION

The Tibetan Plateau (TP) serves as a water tower of Asia and is sensitive to climate change (Li et al., 2022b). Changes in the precipitation over the TP are crucial to the local water storage and affect the freshwater supply to the surrounding regions, as well as local glacier mass balance, lake volume and ecosystems (Piao et al., 2020; Shaw et al., 2022; Yang et al., 2017; Yao et al., 2022). Climate warming over the TP has been observed to be amplified by more than double the global warming rate (Bibi et al., 2018; IPCC, 2013; Yao et al., 2019), accompanied by an overall wetter TP with increases in water vapour content and precipitation (Xu et al., 2008; Yang et al., 2011; Yao et al., 2022). However, the increasing trends in precipitation are not uniform in space, and some regions such as southeastern and southwestern TP have experienced reductions in precipitation in recent decades (Ehlers et al., 2022; Gao et al., 2014). Understanding what processes drive these precipitation changes over the TP is essential to better anticipate and predict future changes in the regional water budget.

Precipitation changes induced by atmospheric processes can be divided into three components: dynamic and thermodynamic contributions, and a covariation term. The thermodynamic contribution is mainly related to changes in atmospheric temperature and moisture, while the dynamic contribution is caused by changes in atmospheric motion. The covariation term represents the changes in the eddy flux and is generally smaller than the other two terms over the TP (Chen et al., 2022; Gao et al., 2014; Wang et al., 2017). In the context of climate warming, the thermodynamic contribution is expected to increase due to increases in saturation specific humidity following the Clausius–Clapeyron relationship (Trenberth et al., 2003). In contrast, how regional precipitation has changed or will change due to changes in the dynamic contribution remains highly uncertain in different regions (Pfahl et al., 2017). Previous studies have attempted to quantify the dynamic, thermodynamic and covariation contributions to precipitation in the TP and surrounding regions using different methods. Zhang et al. (2019b) performed a moisture budget analysis at the gridpoint scale and found that both the dynamic and thermodynamic contributions are important for the precipitation changes over the TP. Generally, the dynamic contribution was found to have led to increased precipitation in the western, northern and southeastern TP, while the positive thermodynamic contributions were larger in the middle and eastern parts of the TP. Gao et al. (2014) found that it is mainly the dynamic contribution that has driven the precipitation changes over the TP during the wet season (May–September).

The dynamic contribution is linked to changes in moisture transport, which has been found to dominate the interannual variability of the summer precipitation over the southern TP (Wang et al., 2017; Zhu et al., 2020). The TP is under the influence of several large-scale flows, including Asian summer monsoons and westerly jets (Bothe et al., 2011; Lai et al., 2021). Summer monsoons are considered to contribute the most precipitation over the TP, while the westerly jets affect precipitation over the western TP during winter (Lai et al., 2021; Maussion et al., 2014; Zhang et al., 2017). Although moisture for TP precipitation comes from a wide area including Eurasia and South Asia, the major differences in moisture contribution between wet and dry years are mainly from South Asia (Zhang et al., 2017). Many studies have focused on the relationships between precipitation over the TP and Asian summer monsoon circulations as well as westerly jets (e.g., Feng & Zhou, 2012; Lai et al., 2021; Maussion et al., 2014). Recent studies also revealed that accurately representing the locations of westerly jets results in improved modelling of summer precipitation in numerical weather models (Ou et al., 2023), highlighting the importance of westerlies for regional precipitation. Most previous studies have treated monsoons or westerly jets as separate circulation systems while few studies have focused on the precipitation resulting from their integrated impacts over time, and the seasonal evolution of the integrated effects (Curio & Scherer, 2016; Zhang et al., 2019a). There is a lack of understanding of how changes in different large-scale circulation patterns have jointly affected the precipitation over the TP.

The large-scale circulation can be described as a continuum of circulation patterns (Franzke & Feldstein, 2005), which can be illustrated using for example a self-organizing map (SOM; Johnson et al., 2008). SOM is an unsupervised machine learning technique commonly used to cluster high-dimensional data to produce a lower-dimensional representation (Kohonen, 1982; Zhang et al., 2018). Liu et al. (2016) used a SOM to relate large-scale circulations and oscillations, such as subtropical highs, monsoons, the El Niño–Southern Oscillation and westerlies, to the seasonality of the precipitation over the TP. Due to their large domain covering a larger part of the entire Northern Hemisphere, their results emphasized synoptic-scale precipitation and circulation patterns and did not clearly show how changes in regional circulations have affected the changes in local precipitation over the TP. Lai et al. (2021) applied the SOM method to regionalize the precipitation over the TP based on its seasonal characteristics and investigated the interannual variations in the precipitation in the different regions and associated circulation patterns. Their results suggest that the regional precipitation has been jointly affected by interannual variations in Asian summer monsoon circulations and westerly jets, but how these circulations have changed and their joint influence on the TP precipitation remains unclear.

This study attempts to explore and quantify the roles of large-scale circulation changes and their joint impacts on regional precipitation over the TP using the ERA5 reanalysis along with the SOM clustering method. The objectives of this study are to (1) identify the continuum of wind patterns over and surrounding the TP, (2) determine the seasonality, interannual variability and trends of the occurrences of the classified circulation and associated precipitation patterns, and (3) quantify the contributions from key large-scale wind patterns by relating the combined changes in Asian summer monsoons and westerlies to regional precipitation changes over the TP.

2 | DATA AND METHODS

2.1 | The ERA5 reanalysis and GPM precipitation

In this study, we focus on the TP within a domain of 25°–45°N and 65°–105°E where most of the area has an elevation exceeding 3000 m. The study is based on the ERA5 reanalysis, which is a fifth-generation atmospheric reanalysis provided by the European Centre for Medium-Range Weather Forecasts (Hersbach et al., 2020). The variables from ERA5 were provided as hourly analysis fields on a 0.25° × 0.25° grid covering 1979–2020.

For the u and v components of the winds at 500 hPa used in the classification, the hourly data were averaged to 5-day (pentad) means to smooth the daily wind fluctuations while preserving a higher temporal resolution than seasonal or monthly averages, resulting in 73 nonoverlapping pentad means starting from 1 January each year (leap days omitted). Several other atmospheric variables from ERA5 were used to explore the atmospheric conditions associated with the classified wind patterns, including the total precipitation, geopotential height and vertical integral of eastward and northward water vapour fluxes. To investigate the relationship between precipitation and thermodynamic/dynamic variables, we used monthly mean convective available potential energy (CAPE), latent heat fluxes, sensible heat fluxes and horizontal divergence (DIV) of the wind field at 500 hPa from ERA5.

To evaluate the ERA5 precipitation, we used satellite-estimated half-hourly precipitation from the Integrated Multi-satellite Retrievals for GPM (IMERG) version 06. We applied the Level 3 product (Huffman et al., 2019) covering the recent two decades (2001–2020) with a spatial resolution of 0.1°. Previous studies have shown that IMERG outperforms other gridded observation and satellite estimates in terms of precipitation amounts over the TP (Kumar et al., 2021; Xu et al., 2017).

2.2 | SOM classification

SOM is a machine learning technique that has been used to classify, among other things, time series of variables, weather patterns and atmospheric circulation patterns in different regions such as the Arctic (Cassano et al., 2007; Chen et al., 2016), Japan (Ohba & Sugimoto, 2021) and the TP (Lai et al., 2021; Liu et al., 2016). With SOM, the classification is performed by first training a map or network of nodes using the input data to produce a low-dimensional representation of the dataset. While the map can be structured in many ways, the most common configuration consists of nodes arranged in a two-dimensional lattice. Because the nodes are connected to adjacent nodes through a neighbourhood function, the trained map preserves the topological structure of the data. After the training phase, data points can be mapped to different nodes by finding the node with the smallest distance to the input.

In this study, we follow the SOM method used by Liu et al. (2016) to identify the dynamic processes from the dominant wind patterns over the TP. First, in the training phase, the SOM was trained using 500 hPa pentad-averaged wind data in the study domain (73 wind maps per year for 42 years) to find a smaller number of representative wind patterns. After the training phase, we used the trained SOM to identify the closest-matching 500 hPa wind pattern for each pentad period based on the Euclidean distance.

To determine which atmospheric level to use for the wind classification, we explored at which level the winds are most strongly related to moisture transport to the TP. Pressure levels below 500 hPa tend to lie below the surface of the high plateau (>4000 m altitude), while at higher levels the moisture transport tends to decrease with height. Thus, we chose to use 500 hPa winds to represent the dynamic motions of wind patterns because they can both represent large circulations for the middle and lower troposphere from outside the plateau and lower tropospheric winds over the plateau.

We determined the optimal SOM size for the classification by performing the SOM clustering for a range of map sizes and calculating, for each SOM size, the mean Euclidean distance between the input data points and the corresponding closest SOM nodes they were mapped to. Following Liu et al. (2016), we applied the Pettitt nonparametric test to look for the change point when increasing the number of nodes did not significantly reduce the mean distance between the input data and the closest SOM nodes. We tested several grid sizes from 2 × 2 to 10 × 10 for the SOM algorithm (Figure S1, Supporting Information) and determined that a total number of 30 (5 × 6) nodes was sufficient to capture the variability in the data.

2.3 | Composite analysis

We conducted composite analyses to investigate how other atmospheric variables, such as precipitation and moisture transport, are related to the wind patterns from the SOM classification. Composites were created by selecting pentad periods that were classified as a particular wind pattern, and then averaging the fields for a particular variable for all selected pentad periods.

Because of the use of pentad data for the full years, the composites often mainly reflect seasonal variations. To reduce the effect of seasonality and focus on the interannual anomalies, we also calculated deseasonalized composites, which were created by first subtracting the 42-year mean seasonal cycle from all pentad fields, and then creating composites using the deseasonalized anomaly fields.

2.4 | Monsoon and westerly indices

Three indices were used to investigate the links between the classified wind patterns and large-scale circulation patterns related to the Indian summer monsoon (ISM), East Asian summer monsoon (EASM) and westerly jets. The ISM index was developed by Wang et al. (2001), derived from the differences in zonal wind speed at 850 hPa between northern India/TP and the Arabian Sea (Figure S2a). We used the ISM index corresponding to the monsoon intensity from June to August during 1979–2019, which can be accessed from the Asia-Pacific Data-Research Center of the International Pacific Research Center at the University of Hawaiʻi at Mānoa (http://apdrc.soest.hawaii.edu/projects/monsoon/seasonal-monidx.html). For the EASM, several indices have been proposed. We used an index proposed by Li and Zeng (2002), which defines the EASM strength based on 850 hPa wind fields within a domain encompassing 10°–40°N and 110°–140°E (Figure S2b), available at http://lijianping.cn/dct/page/65577. Wang et al. (2008) performed a comprehensive assessment of commonly used EASM indices and concluded that over half of the assessed indices were well correlated with the leading mode of EASM variability. In this assessment, the index proposed by Li and Zeng (2002) performed as one of the top 5 indices in terms of capturing the interannual EASM variations. We focused on the summertime (June–August) EASM index values from 1979 to 2020.

Because there is no widely established index for studying the westerlies under the influence of westerly jets over the TP, we considered several definitions used in previous studies to identify a westerly index. For example, Schiemann et al. (2009) and Sha et al. (2020) focused on the seasonality of jet shifts around 20°–50°N above 500 hPa.

Several studies investigated the westerly jets by using existing indices to represent the intensity of the westerlies, such as the Global Teleconnection index that was used to study the area of 35°–40°N and 60°–70°E (Ding & Wang, 2005; Mölg et al., 2017) and the North Atlantic Oscillation index (Liu et al., 2018; You et al., 2011). We explored the seasonality of locations of westerly jets and the sensitivity of different index definitions (Figure S3) and found that the seasonal transition and interannual variability of westerly jets upstream of the TP can be captured by the u-wind in two regions to the southwest and northwest of the TP. Thus, for our application, we chose to quantify the intensity of westerlies using the average u-wind speed between 500 and 100 hPa within these two regions: 23°–35°N and 60°–70°E (the southern westerly index), as well as 35°–47°N and 60°–70°E (the northern westerly index). The values were standardized by subtracting the long-term mean and dividing by one standard deviation. These two indices represent the intensity of upstream westerlies that could result in precipitation events in especially the western and southeastern TP during winter and spring.

2.5 | Partial correlation

We used partial correlation analysis to examine the relationships between regional precipitation over the TP and variables related to dynamic and thermodynamic processes. This method measures the linear relationship between two variables while controlling for the effect of other variables. For variables that have high correlations with each other, we kept only the variable with the highest correlation with precipitation to avoid overlapping explanatory variables. Variables that are not linearly related to precipitation were also excluded from the analysis. In the end, we used CAPE, latent heat flux, sensible heat flux and DIV at 500 hPa in the partial correlation analysis. The climatological seasonal cycles of all variables were subtracted before the correlation analysis.

3 | RESULTS AND DISCUSSION

3.1 | Classified wind patterns and their seasonality

Figure 1 shows the trained SOM for 500 hPa winds in the TP and surrounding regions, and the corresponding geopotential height composites are shown in Figure S4. From left to right, Figure 1a shows a transition from predominantly westerly winds to relatively weak winds over the TP. The top nodes exhibit stronger westerly winds (westerlies) to the north of the plateau, while the bottom
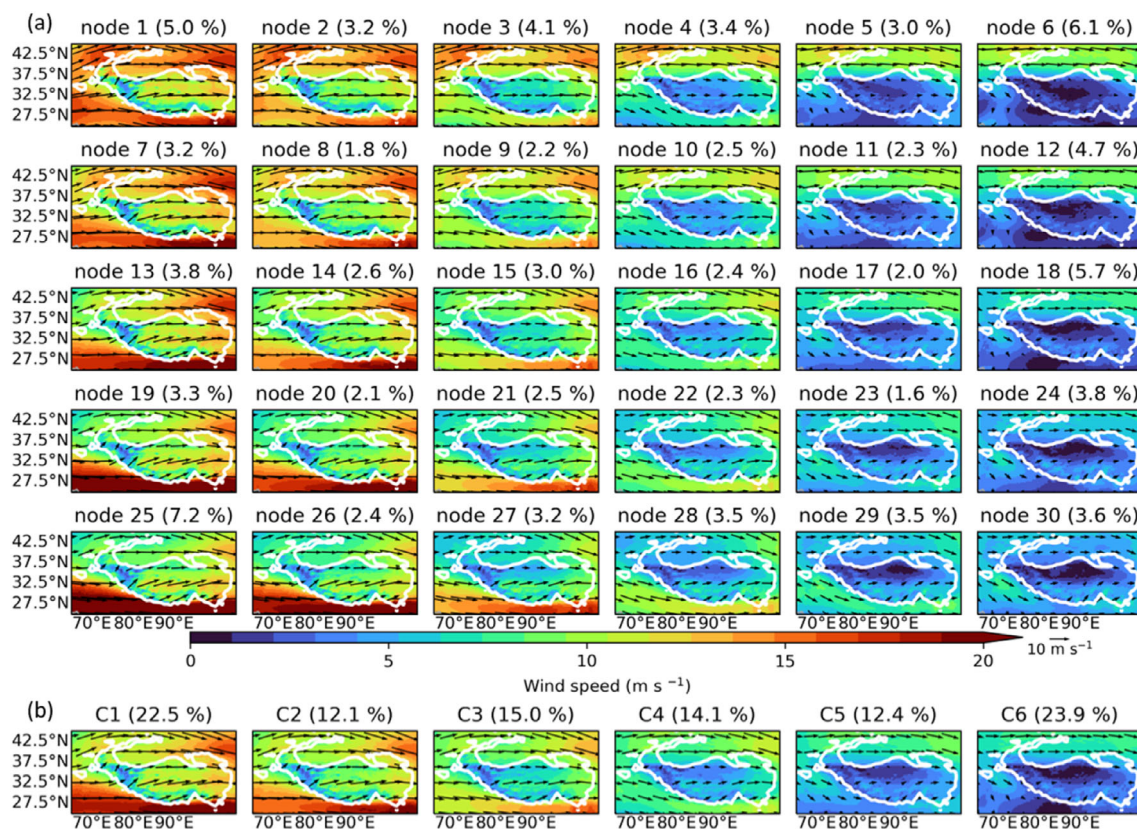
FIGURE 1 (a) SOM clusters representing classified wind patterns in a 5 × 6 grid. The shading denotes the speed of the 500 hPa winds (shown as vectors). The white contour indicates the 3000 m elevation. (b) Composites of the classified wind patterns obtained from each column in (a). The percentages above each cluster indicate the occurrence frequencies of the respective clusters.

nodes reflect stronger westerlies and increased southerly flow into the southern TP. Overall, the associated geopotential heights are lower and with stronger gradients in the left nodes compared with the right nodes (Figure S4), indicating that the left-to-right direction of the SOM partly reflects the seasonality of the wind patterns. To the southwest of the TP, the top-right nodes show an anticyclonic circulation pattern, which is typical for the Asian summer monsoon circulation in this area (Tao et al., 2001), while the left nodes show strong westerlies commonly featured during the winter and transition seasons (Schiemann et al., 2009). Figure 1b shows the average wind patterns and associated geopotential heights for each column in the SOM, highlighting the transition from westerly-dominated to monsoon circulation-dominated features in the southwestern part of the domain.

For each wind pattern, we counted the number of occurrences within the annual cycle for all 42 years. The occurrences of the columns of the SOM show a clear seasonality with the peaks transitioning from winter to summer from the left to the right columns (Figure 2a). The transition seasons spring and fall share the same wind

patterns. The node in the bottom-left corner of the SOM is the dominant wind pattern in winter, while the top-left nodes are more common in early and late winter (Figure 2a). Similarly, the top-right nodes show a prominent peak in the middle of the summer season in July, while the bottom-right nodes mostly occur in early summer.

Figure 3 shows the precipitation and horizontal water vapour flux composites associated with the classified wind patterns. The precipitation patterns reflect mainly the seasonal cycle, with the strongest precipitation in the southeastern TP in summertime (right nodes), and precipitation mainly in the western TP in winter (left nodes). We evaluated the precipitation composites from ERA5 with precipitation from IMERG during 2001–2020. The spatial distributions of IMERG precipitation amounts show similar patterns as ERA5 (Figure S5), except for an overestimation in ERA5 relative to IMERG across the entire TP for all nodes (Figure S6). This wet bias in ERA5 is consistent with the findings from previous studies (e.g., Orsolini et al., 2019). Yuan et al. (2021) pointed out that although ERA5 overestimates the precipitation amount
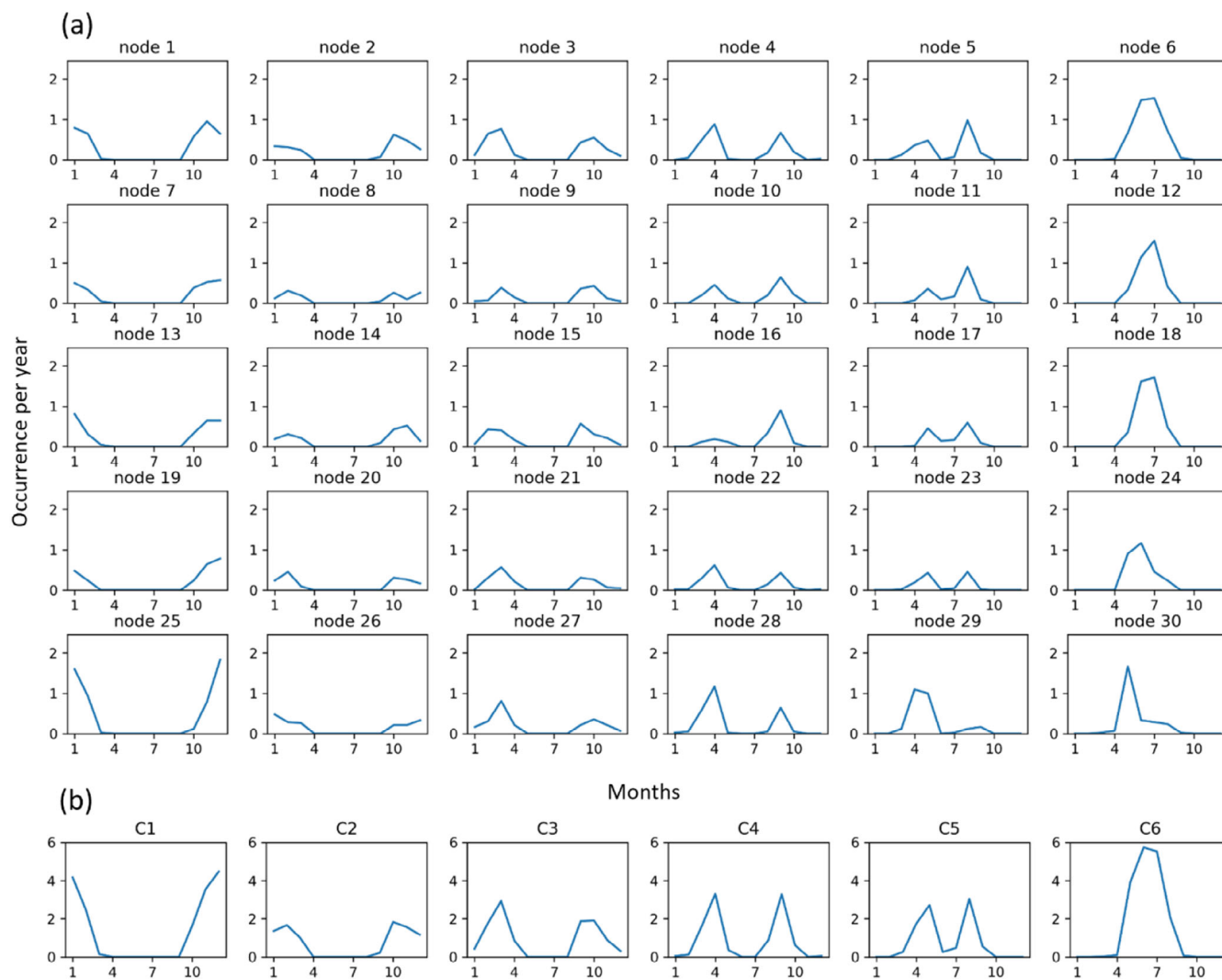
FIGURE 2 (a) Averaged monthly frequency of occurrence of the 5 × 6 SOM clusters over a 42-year period and (b) the summed monthly frequency derived from each column in (a). The pentad data were consolidated based on the closest 15th of each month, resulting in the formation of the monthly series.

in this area compared with observation-based datasets and other downscaling modelling products, it has a better capability for interdecadal studies in terms of spatiotemporal variability of precipitation. Since we are interested in the trends and variability of the relationship between high-resolution circulation patterns and precipitation, ERA5 is considered suitable for our purposes.

To disentangle the distinctive impact of wind patterns from the inherent seasonal cycle, Figure 4 shows the deseasonalized composites of precipitation and horizontal water vapour flux. The leftmost nodes show a dipole of above- and below-average precipitation in the western and eastern TP. Increased precipitation in the western TP is associated with anomalous southwesterly water vapour transport caused by stronger westerlies to the north of

the TP, while the wetting of the eastern TP in the bottom-left nodes is related to increased westerly and southerly winds in the southern TP.

For the wind patterns that occur mainly in summertime (rightmost nodes), the corresponding deseasonalized precipitation composites (Figure 4) show a seesaw pattern between eastern and southwestern TP. The enhanced precipitation in the eastern TP is linked to stronger southerly components of the winds and moisture transport in the southeastern TP. On the other hand, a drier eastern TP and wetter southwestern TP are associated with weaker southerly moisture flux (northerly moisture flux anomalies) in the eastern TP and stronger southeasterly moisture flux anomalies to the southwest of the TP, which is a typical feature of a strong ISM (Tao et al., 2001).
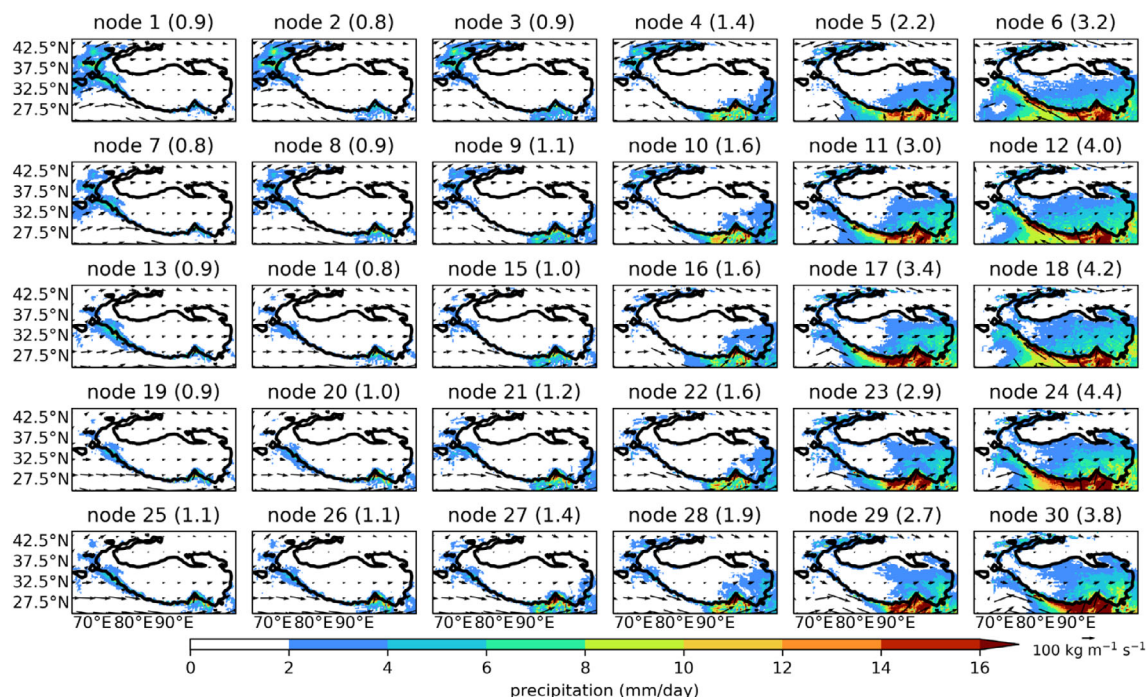
FIGURE 3 SOM clusters illustrating precipitation and vertically integrated horizontal water vapour fluxes from ERA5 in a 5 × 6 arrangement. The values within parentheses above each cluster indicate the average precipitation amount (mm/day) over the TP (within the black contour).
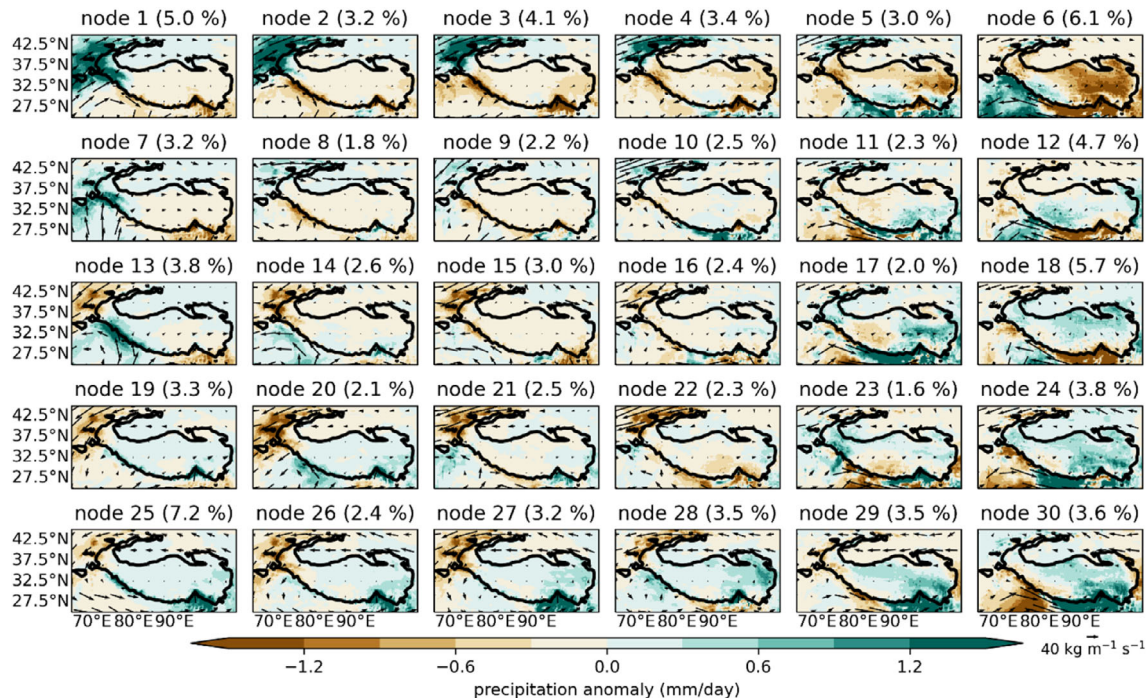

FIGURE 4 Anomalous precipitation (shaded) and vertically integrated horizontal water vapour fluxes (indicated by arrows) based on ERA5, corresponding to the wind patterns in Figure 1. The anomalies for each node were calculated by subtracting the 42-year average seasonal cycle from each pentad precipitation associated with a specific node, followed by averaging all deseasonalized pentad precipitation anomalies. The numbers within parentheses above each cluster represent the frequencies of occurrences of the respective clusters.
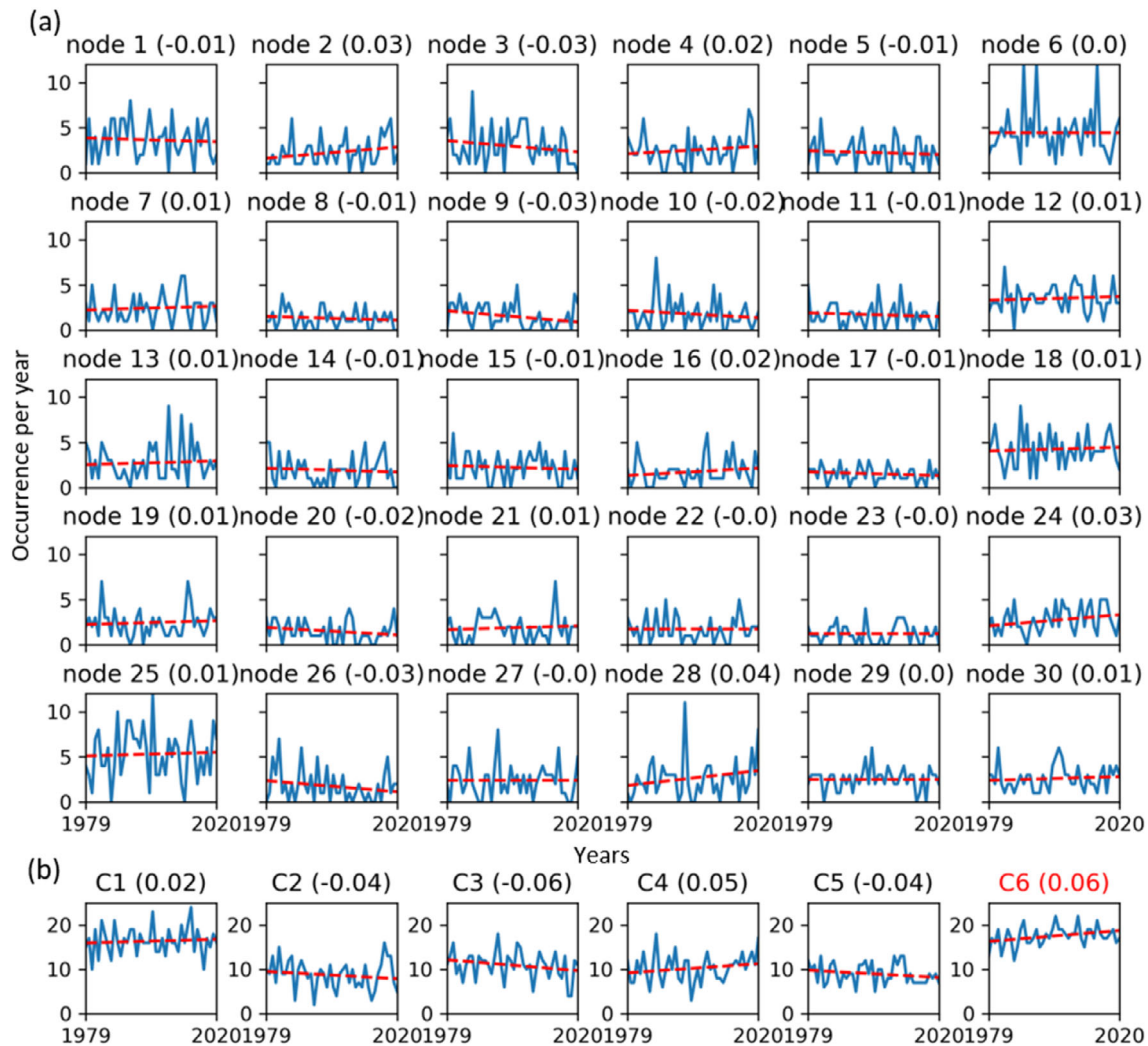
FIGURE 5 Interannual variabilities of the classified 5 × 6 SOM clusters for (a) individual nodes and (b) column sums. The red lines show the trend lines from a linear least-squares regression. The values above each cluster denote the trends (unit: pentad per year) and red text represents $p < 0.05$. The p-values were computed using the Wald Test with t distribution.

During the transition seasons, the main features of the deseasonalized precipitation composites (the middle four columns in Figure 4) are positive or negative precipitation anomalies located over the western and eastern TP. The precipitation anomalies depend on the anomalous moisture fluxes from the west or south of the TP. When the moisture flux anomalies show a strong southwesterly component associated with enhanced westerly winds to the northwest or southeast of the TP, the positive precipitation anomalies tend to be in the northwestern (top middle nodes in Figure 4) and southeastern (bottom middle nodes in Figure 4) TP, respectively. Overall, the dynamic processes related to the different precipitation patterns over the TP are similar between the winter and transition seasons. These results

highlight the importance of the strength and location of westerlies for the precipitation over the TP in these seasons.

3.2 | Interannual variabilities and trends of the classified wind patterns, precipitation and circulation indices

The classified wind patterns in Figure 1 show strong seasonality and their numbers of occurrences also vary considerably between different years (Figure 5). To examine the relationships between the classified wind patterns and precipitation over the TP on an interannual timescale, we first investigated the relationship between the
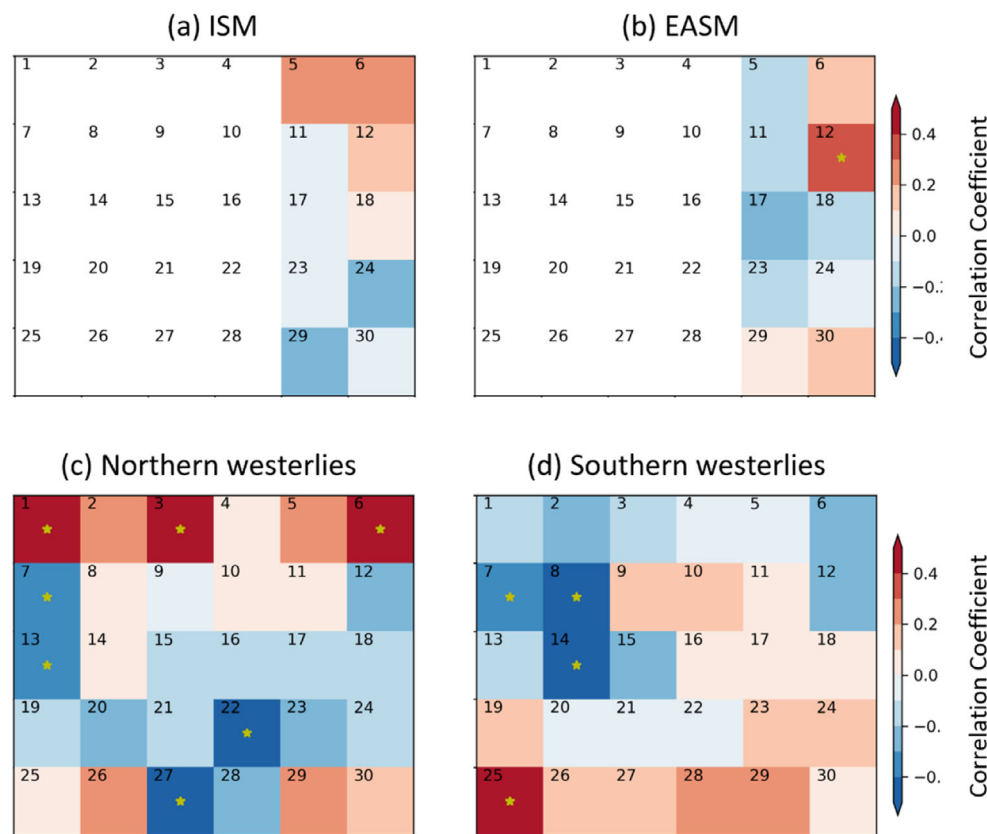
FIGURE 6 Correlation coefficients between the annual frequency of occurrences of each node and the following indices during the periods 1979–2019 for (a) (due to data availability) and 1979–2020 for (b)–(d): (a) Indian summer monsoon (ISM) index, (b) East Asian summer monsoon (EASM) index, (c) the northern westerly index and (d) the southern westerly index. The numbers in the top-left corners denote the node number. The occurrences for the nodes were counted for the months covered by the respective indices (June–August for ISM and EASM in (a, b)). In the case of the westerly indices, correlations were established based on the SOM rainy months for each aggregated group (see Figure 2b), that is, October–February for C1, September–March for C2, September–April for C3, March–May and August–October for C4, March–September for C5 and May–August for C6. Only correlation coefficients derived from sample sizes exceeding 10 are shown. Stars denote significance at $p < 0.05$.

classified wind patterns and known large-scale atmospheric circulations, such as summer monsoons and westerly jets.

To that end, we calculated the interannual correlations between different indices representing the intensities of the summer monsoons (ISM and EASM) and westerlies, and the numbers of occurrences of the wind patterns during the SOM rainy months. The SOM rainy months for each aggregated group were defined according to the months when most of the precipitation occurs (see Figure 2b): October–February for C1, September–March for C2, September–April for C3, March–May and August–October for C4, March–September for C5 and May–August for C6. The number of occurrences of the top-right nodes is positively correlated with the interannual variabilities of the ISM and EASM intensities, but only the correlation with EASM is significant (node 12; see Figure 6). Nodes 5 and 6 are positively correlated with the ISM intensity, associated with anomalous

southwesterly moisture fluxes to the southwest of the TP. Lai et al. (2021) showed a similar relationship between a stronger ISM and southwesterly moisture fluxes, indicating that the classified wind patterns from this study can represent to some degree the strength of the ISM circulation.

Whether and to what extent the strength of the EASM affects the precipitation over the TP remains an open question (e.g., Curio et al., 2015; Du et al., 2020; Lai et al., 2021). Our results show that the occurrence of the summer-wind pattern in node 12 is significantly and positively correlated to the interannual EASM strength changes (Figure 6b). The occurrences of the other 4 nodes (nodes 6, 18, 24, 30) in the C6 summer-wind group are however not statistically significantly ($p > 0.05$) correlated to the interannual variability of the EASM strength. Although more studies should be carried out to further examine the impacts of the EASM on the TP precipitation, the significantly positive correlation between
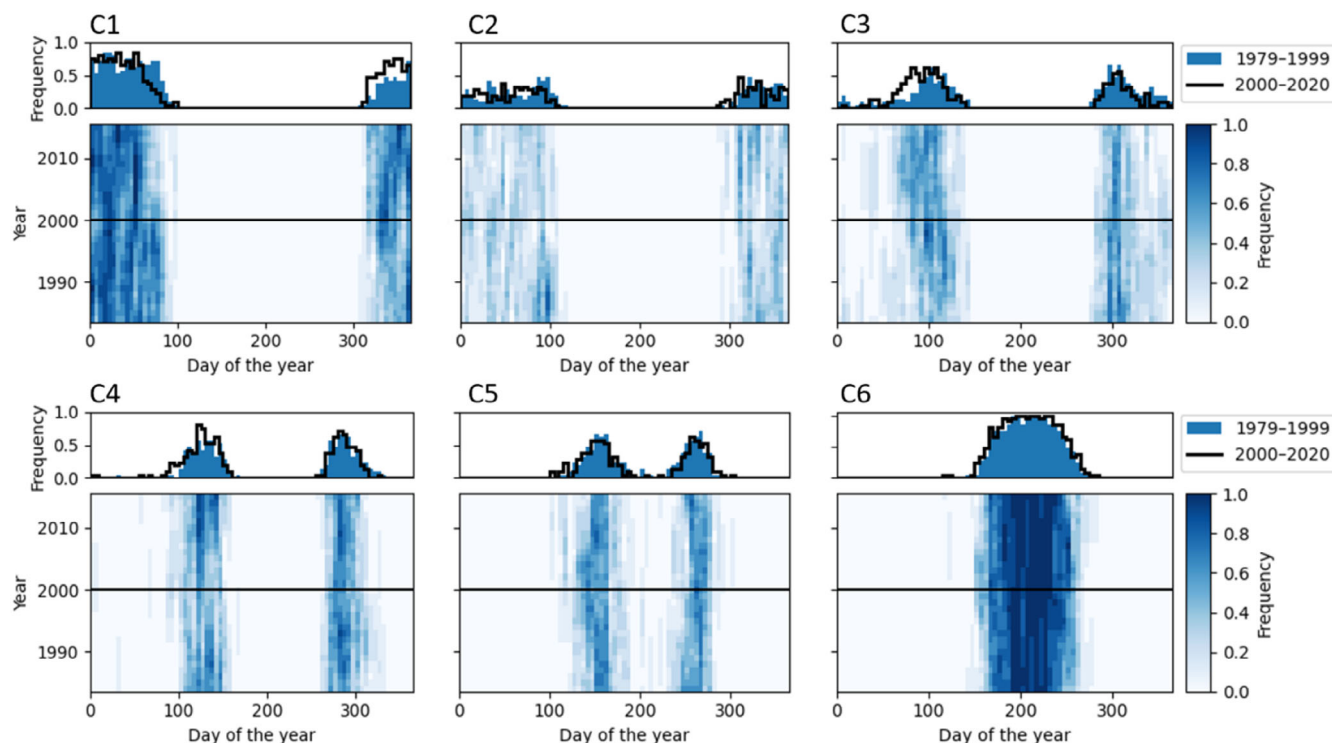
FIGURE 7   Frequency of occurrence of SOM nodes corresponding to the aggregated classified wind patterns C1–C6 as depicted in Figure 1. The upper panel in each subplot presents the mean frequency of occurrence during 1979–1999 (depicted by blue bars) and 2000–2020 (illustrated as black lines). The lower panels illustrate the average frequency of occurrence using 11-year centred moving windows, with black horizontal lines demarcating the two periods in the upper plots.

the EASM strength and classified wind pattern suggests that a stronger EASM is linked to enhanced precipitation over the central and eastern TP (Figure 4).

The westerly index that displays the strongest relationship with the wind patterns is the one reflecting the intensity of the westerlies to the southwest of the TP (Figure 6d), especially in the nodes that mainly occurred in winter. Increased occurrences of nodes 1, 3 and 6 are significantly positively correlated with stronger westerlies to the northwest of the TP (Figure 6c). Significant negative correlations are found for nodes in the middle rows where the weakened westerlies are associated with anomalous northeasterly and cyclonic moisture fluxes to the northwest and southwest of the TP, respectively (Figure 4). Overall, the classified wind patterns can well capture the characteristics of the westerlies upstream of the TP.

The significant correlations between the occurrences of the wind patterns and TP precipitation on the interannual timescale (Figure 6) raise the question of whether there are any trends in the occurrences of the wind patterns. While no individual wind pattern shows a significant trend from 1979 to 2020 (Figure 5a), when considering all summer wind patterns in the last column of the SOM (C6 in Figure 1), we find a significant upward

trend of 0.6 pentads·decade^{-1} ($p < 0.05$) (Figure 5b). None of the other column-aggregated wind patterns show significant trends in their annual numbers of occurrences.

To more closely examine how the wind patterns have changed within the year, Figure 7 shows the frequencies of occurrences of the column-aggregated wind patterns as a function of the day of the year. To smooth out the strong interannual variations, we calculated the frequencies of occurrences over an 11-year moving window. The top panels of the subplots in Figure 7 also illustrate the changes in frequencies of occurrences between 1979–1999 and 2000–2020. C6 in Figure 7 reveals that the positive trend in the occurrence of the summer wind pattern is due to both an earlier onset and a later demise of this wind pattern, which is considerably affected by monsoons. Previous studies found that the declining intensity of the EASM has recently recovered (Zhang, 2015) and is projected to become stronger in the future (Li et al., 2022a). The strengthening of the EASM is projected to accompany increasing precipitation under future climate warming (Li et al., 2019). Looking at the individual summer wind patterns in C6, all nodes except node 6 show positive trends (Figure 5). Given that the wind patterns with positive trends are associated with

increased precipitation over the TP (Figure 4), our result shows that the increased frequency of occurrence of the summer wind patterns has likely led to a wetter TP.

The aggregated wind patterns C3–C5 occurring in the transition seasons show an advancing start date in the first half of the year, which could be associated with warmer springs over the TP (UNEP, 2022). For the C1 wind pattern representing the dominant winter circulation, there is a clear trend toward a more frequent occurrence in late fall and early winter, and a decreased frequency of occurrence in late winter. The increase (decrease) in C1 is mostly explained by a corresponding decrease (increase) in C3. Because the C1–C4 wind patterns are under the influence of the westerlies (Figure 1b), the movement and interannual variability of the westerlies could have a major impact on the trends of the wind patterns. Overall, the midlatitude westerly jets in the Northern Hemisphere have been found to have shifted poleward (Archer & Caldeira, 2008). Although some studies have suggested that the interannual variability of the jet locations around the TP is small (Schiemann et al., 2009; Zhang & Huang, 2011), a recent study by Zhou et al. (2022) shows that the westerly jet is projected to be moving equatorward in the region of Asia-Pacific during the early summer. The warmer spring over the TP (UNEP, 2022) and shifts in the westerlies could partly explain the changes in the occurrences of the C1 and C3 wind patterns. We examined the difference in early springtime geopotential height, u-wind and temperature between the earlier and later 21 years (1979–1999 and 2000–2020) and found a positive anomalous geopotential height to the northwest of the TP in the later period (Figure S7a). This geopotential height difference indicates weakened westerlies in the later decades, which could be due to weaker meridional temperature gradients (Figure S7b) and earlier northward shifting in westerly jets. Therefore, the advancing start date of the springtime wind pattern could occur more often due to warmer spring to the northwest of the TP. More studies are needed to explore the mechanism for the trends in westerly jets during different seasons.

3.3 | Contributions from large-scale wind patterns and other variables to regional precipitation changes

To further understand the impacts of the classified wind patterns, as well as other variables on regional TP precipitation, we focused on three regions with distinct seasonal precipitation and climate characteristics identified by Lai et al. (2021) and used by Slättberg et al. (2022), which are located in the western, central and eastern TP

(see Figure 8a). Based on the previous two studies, the wet seasons of the three regions occur from January to April in the western TP, July to September in the central TP and May to October in the eastern TP.

Figure 8b–d shows the correlations between the annual occurrences of the nodes and the annual precipitation anomalies after subtracting the climatological seasonal cycles in the three regions. The wet-season (mainly winter) precipitation in the western TP is positively associated with the top-left wind patterns in the SOM, which shows that the precipitation in this region is significantly affected by the dynamics of the westerly jets to the north of the TP. On the other hand, the western TP experiences a drier wet season when the anomalous southwestern moisture fluxes to the southwest of the TP are strengthened, or when the westerlies to the north of the TP are weakened. The results indicate that the precipitation in the western TP strongly depends on the strength and locations of the stronger westerlies relative to the climatological mean.

The wet-season anomalous precipitation in the central TP is significantly positively correlated to the frequency of occurrence of the classified wind pattern in node 12 with relatively stronger southeasterly moisture fluxes in July (Figure 8c). This node was previously found to be related to the EASM intensity (Figure 6b). Conversely, anomalous northwesterly moisture fluxes to the south of the TP associated with the wind patterns in nodes 11 and 23 in the transition seasons are associated with a relatively dry central TP. No significant correlations were found with the nodes related to the ISM. This lack of correlation does not necessarily mean that the precipitation in central TP is not affected by the ISM, as previous studies have suggested that the ISM is the main source of moisture supply in this region (Ma et al., 2018). Although the EASM is usually thought to affect the precipitation in the eastern TP (e.g., Du et al., 2020), a few studies have also shown that a weakening EASM could be associated with the increased precipitation to the north of the TP through water vapour transport (Chen et al., 2021a, 2021b). Our results show that the EASM might be one of the factors that have affected the interannual variability of the precipitation in the central TP. Further research is needed to determine the mechanisms behind the link between the EASM and precipitation in the central TP.

Precipitation in the eastern TP was more closely related to the classified wind patterns with stronger westerly jets and westerlies to the south of the TP (nodes 17 and 21) and also with a slight anomalous southerly component of moisture fluxes in the eastern TP (nodes 27–30) during the transition seasons (Figure 8d). On the other hand, the eastern TP was generally drier when
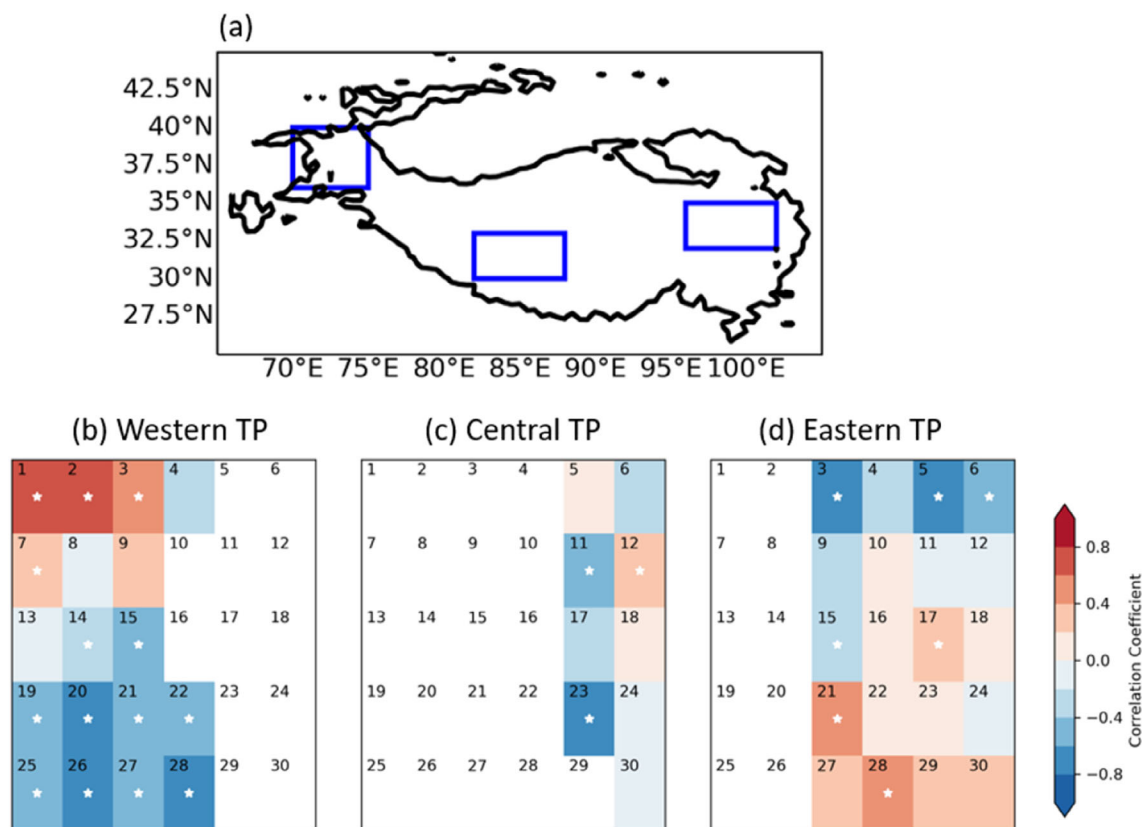
FIGURE 8 (a) Geographical representation highlighting the analysed subregions (marked with blue boxes). From left to right: the western TP, central TP and eastern TP. The lower panels show the correlation coefficients between annual node occurrences and precipitation anomalies (for the wet season), after subtracting the climatological seasonal cycle, in the (b) western TP (January–April), (c) central TP (July–September) and (d) eastern TP (May–October). Only correlation coefficients calculated from sample sizes exceeding 10 are shown. Significance is indicated by stars (*), denoting $p < 0.05$.

the wind patterns related to the ISM occurred (nodes 5 and 6), or when the westerlies to the north of the TP were stronger than the average westerlies (node 3) during the transition seasons. The precipitation in the eastern TP is influenced by the EASM and local convection during the transition and Asian summer monsoon seasons (Curio et al., 2015). Schiemann et al. (2009) showed that the meridionally shifting of the westerly jets could be associated with the precipitation distribution in the northwestern and eastern TP. Our analysis shows that it is not only the monsoons that affect the interannual variability of the precipitation in the eastern TP, but the location of the westerly jets and strong westerlies also plays a crucial role in the regional precipitation distribution.

Although the wet-season precipitation over the central and eastern TP is usually attributed to the influence of monsoon systems, the precipitation recycling from local evaporation could have contributed a large portion of the moisture to the regional precipitation (Zhao & Zhou, 2021). As Figure 8 shows, the variations in precipitation over particularly the central TP are not well explained by variations in the classified wind patterns. To

find an alternative explanation for the precipitation vacations in the central and eastern TP, we examined the partial correlations between the regional precipitation and regionally averaged atmospheric variables: CAPE, latent heat fluxes, sensible heat fluxes and DIV at 500 hPa.

Table 1 lists the partial correlations between the interannual variability in precipitation and the four atmospheric variables in the three regions during their respective wet seasons. In the western TP, local convection is shown to be highly correlated to this region's interannual variabilities of precipitation. When calculating the correlations between the precipitation and CAPE only, the coefficient is about 0.22, and increases to 0.70 when controlling for latent heat flux. Because the CAPE variations are small (values around 5–10 J·kg^{-1}), the importance of CAPE on the precipitation variations should be limited. The positive high correlation with latent heat flux suggests that stronger precipitation in the western TP leads to enhanced condensation at the surface. In the central TP, all examined variables (CAPE, latent heat flux and sensible heat flux) except DIV are significantly correlated to the precipitation. The results

TABLE 1 Partial correlations between interannual variability in precipitation and four atmospheric variables during the wet seasons: January–April for the western TP, July–September for the central TP and May–October for the eastern TP

Interannual partial correlations	CAPE	DIV	LHF	SHF
Western TP	0.73*	0.06	0.72*	−0.17
Central TP	0.69*	−0.29	−0.38*	0.65*
Eastern TP	0.36*	−0.35*	−0.04	0.08

Note: The four atmospheric variables are convective available potential energy (CAPE, $J \cdot kg^{-1}$), horizontal divergences of the wind at 500 hPa (DIV, s^{-1}; negative for convergence), latent heat fluxes (LHF, $W \cdot m^{-2}$; negative for evaporation) and sensible heat fluxes (SHF, $W \cdot m^{-2}$; negative for upward fluxes) averaged over the three studied subregions shown in Figure 8a during their corresponding wet seasons. The climatological seasonal cycles of all variables were subtracted before the correlation analysis. Asterisks (*) represent $p < 0.05$.

suggest that convection and evaporation could be important to the interannual variability of precipitation production in this part of the TP. In the eastern TP, DIV at 500 hPa and CAPE contributed roughly equally to the interannual variations in the regional precipitation, which indicates the importance of the interactions between winds and local convections to the precipitation in this region. Here we quantified the importance of both wind patterns and local surface heating (e.g., CAPE) to regional precipitation. As we have shown the trends and interannual variabilities in wind patterns, future studies focusing on long-term changes in local processes are essential to further understand the precipitation variability across the TP.

4 | DISCUSSION

Here we applied SOM to examine how changes in the large-scale circulation patterns have affected the precipitation over the TP. While some studies considered the changes in the occurrences of SOM nodes as dynamic contributions to precipitation changes (e.g., Cassano et al., 2007; Ohba & Sugimoto, 2021), this might not be applicable over the TP because some small-scale wind patterns caused by complex terrain were not fully captured by the SOM classification. We compared the results from the SOM analysis with the results from a traditional moisture budget analysis (from Gao et al., 2014; Zhang et al., 2019b) and found that the SOM method indicated smaller dynamic contributions over the eastern and northeastern TP (not shown). While the quantification of the dynamic and thermodynamic contributions to precipitation through the moisture budget equation may be physically explainable, it is challenging to connect the results to changes in large-scale circulation patterns. Here we are interested in how the interannual variability and trends in large-scale and regional circulation patterns related to monsoons and westerlies under the background of climate change have affected the precipitation

over the TP. Hence, our study focuses on the contributions from the classified large-scale and regional wind patterns as a first step, and further analysis could explore the dynamic processes and their importance for the regional TP precipitation.

The findings from this study show the important role of westerlies in TP precipitation variations. Many previous studies have focused on the relationships between variations of monsoons and changes in precipitation, as monsoons can bring a large amount of moisture to the TP, and are therefore often considered a key factor for the precipitation over the TP. In contrast, the influence of westerly jets on TP precipitation has received less attention. Our results indicate that the shifting locations of westerly jets and strong westerlies are one of the dominant features. Moreover, regions under the influence of anomalously strong westerlies tend to experience enhanced precipitation in winter and transition seasons. Another important finding from this study is the temporal continuum of wind patterns from winter to summer. While most studies have focused on the variations of one particular large-scale circulation system and the related spatiotemporal precipitation anomalies, we show the continuum of maps of wind patterns from different large-scale circulations and their precipitation patterns, as well as their interannual variations.

To what extent horizontal moisture originates from outside or inside the TP is of importance for understanding the regional hydrological budget. Zhao and Zhou (2021) showed that the inner water cycle over the TP could contribute to 23% of the summer precipitation. More than half of the increasing trends of summer water vapour over the TP have also been found to originate from the inner water cycle (He et al., 2021). With their findings of changes in moisture source from outside or inside the TP in mind, we related the variations of the precipitation specifically to different types of wind patterns and their combined influences. Our results point out that the westerly jets and westerlies are important to the variations of the precipitation not only in the western TP but also in the eastern TP. The Asian summer

monsoons may also influence the precipitation in regions that have generally been considered to be less influenced by monsoons, such as the EASM and precipitation over the central TP. Future work could include methods such as moisture tracking (e.g., Cheng & Lu, 2020; Zhang et al., 2017) to physically identify the main moisture sources for different TP regions.

Our study identified the wind patterns with 500 hPa winds. This has been assessed according to the level of strong water vapour transportation. Recent studies have shown that the major inputs of water vapour transportation are concentrated below 700 hPa from the southern boundaries, and between 400 and 700 hPa at the western and eastern boundaries of the TP (Feng & Zhou, 2012; Sun et al., 2022). Our choice at 500 hPa is a bit higher for the water vapour from the southern boundaries but within the layers for the western and eastern boundaries. On the other hand, it has also been reported that the surface pressures of the TP are about 300–500 hPa (Yan et al., 2020). A choice of pressure below 500 hPa is not suitable for studying the wind patterns over the TP. Sun et al. (2022) showed that the major water vapour transportation is at about 500 hPa over the southern TP. Therefore, using 500 hPa wind in the classification cannot fully represent the maximum water vapour transportation over the whole domain, but is an optimal choice to include the most water vapour transportation in both the TP and adjacent regions.

5 | SUMMARY AND CONCLUSIONS

The overall aim of this study was to probe into the transformations within large-scale circulations and their collective impacts on the changes in precipitation over the TP. First, we identified the most frequently occurring wind patterns over and around the TP using ERA5 500 hPa winds and the SOM classification method. Next, we examined the variations and changes in the wind patterns including the long-term trends, seasonality and variabilities in their yearly occurrences and start/end dates. We then calculated the correlations between the frequencies of occurrence of the wind patterns and indices of monsoons and westerlies. Finally, we analysed the relationships between the regional precipitation in three different regions with distinctive seasonalities of precipitation—western, central and eastern TP—and the wind patterns, as well as different atmospheric variables.

The main results and findings from this study are as follows:

1. The classified wind patterns reveal that the seasonal migration of the winds was dictated by stronger westerlies shifting from the north to the south of the TP, along with overall stronger westerly jets in winter and monsoon circulations in summer. With the shifting westerly jets from the north to the south of the TP, the locations of positive anomalous precipitation occurred accordingly from the western TP to the southeastern TP during the winter. In the transition seasons, the classified maps also show the combined influences of the monsoons and westerlies on the spatial distribution of the precipitation. The locations of anomalous precipitation were mainly controlled by the locations of the westerly jets. During the summer, there are seesaw patterns of positive and negative anomalous precipitation between the eastern and southwestern TP due to the location of moisture flux convergences.

2. The locations of abundant precipitation during the winter and transition seasons are strongly linked to the interannual variations in the intensity of the westerly jets. The results suggest the importance of the intensity and location of the westerly jets in determining the interannual variability of the precipitation over the TP.

3. Overall, there were no significant trends in the occurrence of wind patterns during 1979–2020. However, when considering all summer-type wind patterns, there was a statistically significant ($p < 0.05$) upward trend of 0.6 pentads·decade^{-1}, which could lead to a wetter TP. In addition, our results show a trend toward an earlier end of the winter wind patterns, and an earlier start of the spring wind patterns, which is likely associated with an overall warmer spring in the context of TP warming.

4. For the regional precipitation, the locations of the westerly jets mainly dominated the precipitation variability in the western TP during the winter and transition seasons. Strong westerly jets in the northern TP are highly correlated with positive anomalous precipitation amounts in the western TP.

5. For the eastern TP, the interannual variations in the precipitation were more closely associated with the locations of the stronger westerlies than the monsoon circulations. During the wet season of the region, increased precipitation was related to stronger southwesterly moisture fluxes that brought more water vapour into this region.

6. In the central TP, the precipitation was associated with wind patterns related to the EASM. Our results show a statistical link between the interannual variability of the precipitation in the central TP and the EASM. The roles of thermodynamic processes (CAPE and latent heat release from the surface) play a larger role in the interannual variability of precipitation during the wet seasons in the central TP than in the other regions.

DATA AVAILABILITY STATEMENT

The data that support the findings of this study are available from the corresponding author upon reasonable request.

ORCID

Hui-Wen Lai https://orcid.org/0000-0003-3813-0276
Deliang Chen https://orcid.org/0000-0003-0288-5618
Hans W. Chen https://orcid.org/0000-0002-8601-6024

REFERENCES

Archer, C.L. & Caldeira, K. (2008) Historical trends in the jet streams. *Geophysical Research Letters*, 35(8), L08803. Available from: https://doi.org/10.1029/2008GL033614

Bibi, S., Wang, L., Li, X., Zhou, J., Chen, D. & Yao, T. (2018) Climatic and associated cryospheric, biospheric, and hydrological changes on the Tibetan Plateau: a review. *International Journal of Climatology*, 38, e1–e17. Available from: https://doi.org/10.1002/joc.5411

Bothe, O., Fraedrich, K. & Zhu, X. (2011) Large-scale circulations and Tibetan Plateau summer drought and wetness in a high-resolution climate model. *International Journal of Climatology*, 31(6), 832–846. Available from: https://doi.org/10.1002/joc.2124

Cassano, J.J., Uotila, P., Lynch, A.H. & Cassano, E.N. (2007) Predicted changes in synoptic forcing of net precipitation in large Arctic river basins during the 21st century. *Journal of Geophysical Research Biogeosciences*, 112(G4), G04S49. Available from: https://doi.org/10.1029/2006JG000332

Chen, C., Zhang, X., Lu, H., Jin, L., Du, Y. & Chen, F. (2021a) Increasing summer precipitation in arid Central Asia linked to the weakening of the East Asian summer monsoon in the recent decades. *International Journal of Climatology*, 41(2), 1024–1038. Available from: https://doi.org/10.1002/joc.6727

Chen, F., Chen, J. & Huang, W. (2021b) Weakened East Asian summer monsoon triggers increased precipitation in Northwest China. *Science China Earth Sciences*, 64(5), 835–837. Available from: https://doi.org/10.1007/s11430-020-9731-7

Chen, H.W., Alley, R.B. & Zhang, F. (2016) Interannual arctic sea ice variability and associated winter weather patterns: a regional perspective for 1979–2014. *Journal of Geophysical Research*, 121(24), 14433–14455. Available from: https://doi.org/10.1002/2016JD024769

Chen, Q., Ge, F., Jin, Z. & Lin, Z. (2022) How well do the CMIP6 HighResMIP models simulate precipitation over the Tibetan Plateau? *Atmospheric Research*, 279, 106393. Available from: https://doi.org/10.1016/j.atmosres.2022.106393

Cheng, T.F. & Lu, M. (2020) Moisture source–receptor network of the east asian summer monsoon land regions and the associated atmospheric steerings. *Journal of Climate*, 33(21), 9213–9231. Available from: https://doi.org/10.1175/JCLI-D-19-0868.1

Curio, J., Maussion, F. & Scherer, D. (2015) A 12-year high-resolution climatology of atmospheric water transport over the Tibetan Plateau. *Earth System Dynamics*, 6(1), 109–124. Available from: https://doi.org/10.5194/esd-6-109-2015

Curio, J. & Scherer, D. (2016) Seasonality and spatial variability of dynamic precipitation controls on the Tibetan Plateau. *Earth System Dynamics*, 7(3), 767–782. Available from: https://doi.org/10.5194/esd-7-767-2016

Ding, Q. & Wang, B. (2005) Circumglobal teleconnection in the northern hemisphere summer. *Journal of Climate*, 18(17), 3483–3505. Available from: https://doi.org/10.1175/JCLI3473.1

Du, W., Kang, S., Qin, X., Ji, Z., Sun, W., Chen, J. et al. (2020) Can summer monsoon moisture invade the Jade Pass in northwestern China? *Climate Dynamics*, 55(11–12), 3101–3115. Available from: https://doi.org/10.1007/s00382-020-05423-y

Ehlers, T.A., Chen, D., Appel, E., Bolch, T., Chen, F., Diekmann, B. et al. (2022) Past, present, and future geo-biosphere interactions on the Tibetan Plateau and implications for permafrost. *Earth-Science Reviews*, 234, 104197. Available from: https://doi.org/10.1016/j.earscirev.2022.104197

Feng, L. & Zhou, T. (2012) Water vapor transport for summer precipitation over the Tibetan Plateau: multidata set analysis. *Journal of Geophysical Research: Atmospheres*, 117(D20), D20114. Available from: https://doi.org/10.1029/2011JD017012

Franzke, C. & Feldstein, S.B. (2005) The continuum and dynamics of Northern Hemisphere teleconnection patterns. *Journal of the Atmospheric Sciences*, 62(9), 3250–3267. Available from: https://doi.org/10.1175/JAS3536.1

Gao, Y., Cuo, L. & Zhang, Y. (2014) Changes in moisture flux over the Tibetan Plateau during 1979–2011 and possible mechanisms. *Journal of Climate*, 27(5), 1876–1893. Available from: https://doi.org/10.1175/JCLI-D-13-00321.1

He, Y., Tian, W., Huang, J., Wang, G., Ren, Y., Yan, H. et al. (2021) The mechanism of increasing summer water vapor over the Tibetan Plateau. *Journal of Geophysical Research: Atmospheres*, 126(10), e2020JD034166. Available from: https://doi.org/10.1029/2020JD034166

Hersbach, H., Bell, B., Berrisford, P., Hirahara, S., Horányi, A., Muñoz-Sabater, J. et al. (2020) The ERA5 global reanalysis. *Quarterly Journal of the Royal Meteorological Society*, 146(730), 1999–2049. Available from: https://doi.org/10.1002/qj.3803

Huffman, G.J., Stocker, E.F., Bolvin, D.T., Nelkin, E.J. & Tan, J. (2019) In: Savtchenko, A. (Ed.) *GPM IMERG Final Precipitation L3 1 day 0.1° × 0.1° V06*. Greenbelt, MD: Goddard Earth Sciences Data and Information Services Center (GES DISC).

IPCC. (2013) Summary for policymakers. In: Stocker, T.F., Qin, D., Plattner, G.-K., Tignor, M., Allen, S.K., Boschung, J. et al. (Eds.) *Climate change 2013: the physical science basis. Contribution of working group I to the fifth assessment report of the intergovernmental panel on climate change.* Cambridge and New York, NY: Cambridge University Press.

Johnson, N.C., Feldstein, S.B. & Tremblay, B. (2008) The continuum of Northern Hemisphere teleconnection patterns and a description of the NAO shift with the use of self-organizing maps. *Journal of Climate*, 21(23), 6354–6371. Available from: https://doi.org/10.1175/2008JCLI2380.1

Kohonen, T. (1982) Self-organized formation of topologically correct feature maps. *Biological Cybernetics*, 43(1), 59–69. Available from: https://doi.org/10.1007/BF00337288

Kumar, M., Hodnebrog, Ø., Sophie Daloz, A., Sen, S., Badiger, S. & Krishnaswamy, J. (2021) Measuring precipitation in eastern Himalaya: ground validation of eleven satellite, model and gauge interpolated gridded products. *Journal of Hydrology*, 599, 126252. Available from: https://doi.org/10.1016/j.jhydrol.2021.126252

Lai, H.-W., Chen, H.W., Kukulies, J., Ou, T. & Chen, D. (2021) Regionalization of seasonal precipitation over the Tibetan Plateau and associated large-scale atmospheric systems. *Journal of Climate*, 34(7), 2635–2651. Available from: https://doi.org/10.1175/JCLI-D-20-0521.1

Li, J. & Zeng, Q. (2002) A unified monsoon index. *Geophysical Research Letters*, 29(8), 115-1–115-4. Available from: https://doi.org/10.1029/2001GL013874

Li, T., Wang, Y., Wang, B., Ting, M., Ding, Y., Sun, Y. et al. (2022a) Distinctive South and East Asian monsoon circulation responses to global warming. *Science Bulletin*, 67(7), 762–770. Available from: https://doi.org/10.1016/j.scib.2021.12.001

Li, X., Long, D., Scanlon, B.R., Mann, M.E., Li, X., Tian, F. et al. (2022b) Climate change threatens terrestrial water storage over the Tibetan Plateau. *Nature Climate Change*, 12(9), 801–807. Available from: https://doi.org/10.1038/s41558-022-01443-0

Li, Z., Sun, Y., Li, T., Ding, Y. & Hu, T. (2019) Future changes in East Asian summer monsoon circulation and precipitation under 1.5 to 5°C of warming. *Earth's Futures*, 7(12), 1391–1406. Available from: https://doi.org/10.1029/2019EF001276

Liu, W., Wang, L., Chen, D., Tu, K., Ruan, C. & Hu, Z. (2016) Large-scale circulation classification and its links to observed precipitation in the eastern and central Tibetan Plateau. *Climate Dynamics*, 46, 3481–3497. Available from: https://doi.org/10.1007/s00382-015-2782-z

Liu, Y., Chen, H., Wang, H. & Qiu, Y. (2018) The impact of the NAO on the delayed break-up date of lake ice over the southern Tibetan Plateau. *Journal of Climate*, 31(22), 9073–9086. Available from: https://doi.org/10.1175/JCLI-D-18-0197.1

Ma, Y., Lu, M., Chen, H., Pan, M. & Hong, Y. (2018) Atmospheric moisture transport versus precipitation across the Tibetan Plateau: a mini-review and current challenges. *Atmospheric Research*, 209, 50–58. Available from: https://doi.org/10.1016/j.atmosres.2018.03.015

Maussion, F., Scherer, D., Mölg, T., Collier, E., Curio, J. & Finkelnburg, R. (2014) Precipitation seasonality and variability over the Tibetan Plateau as resolved by the high Asia reanalysis. *Journal of Climate*, 27, 1910–1927. Available from: https://doi.org/10.1175/JCLI-D-13-00282.1

Mölg, T., Maussion, F., Collier, E., Chiang, J.C.H. & Scherer, D. (2017) Prominent midlatitude circulation signature in High

Asia's surface climate during monsoon. *Journal of Geophysical Research: Atmospheres*, 122(23), 12702–12712. Available from: https://doi.org/10.1002/2017JD027414

Ohba, M. & Sugimoto, S. (2021) Dynamic and thermodynamic contributions of ENSO to winter precipitation in Japan: frequency and precipitation of synoptic weather patterns. *Climate Dynamics*, 59, 1489–1504. Available from: https://doi.org/10.1007/s00382-021-06052-9

Orsolini, Y., Wegmann, M., Dutra, E., Liu, B., Balsamo, G., Yang, K. et al. (2019) Evaluation of snow depth and snow cover over the Tibetan Plateau in global reanalyses using in situ and satellite remote sensing observations. *Cryosphere*, 13(8), 2221–2239. Available from: https://doi.org/10.5194/tc-13-2221-2019

Ou, T., Chen, D., Tang, J., Lin, C., Wang, X., Kukulies, J. et al. (2023) Wet bias of summer precipitation in the northwestern Tibetan Plateau in ERA5 is linked to overestimated lower-level southerly wind over the plateau. *Climate Dynamics*, 61, 2139–2153. Available from: https://doi.org/10.1007/s00382-023-06672-3

Pfahl, S., O'Gorman, P.A. & Fischer, E.M. (2017) Understanding the regional pattern of projected future changes in extreme precipitation. *Nature Climate Change*, 7(6), 423–427. Available from: https://doi.org/10.1038/nclimate3287

Piao, S., Wang, X., Park, T., Chen, C., Lian, X., He, Y. et al. (2020) Characteristics, drivers and feedbacks of global greening. *Nature Reviews Earth & Environment*, 1(1), 14–27. Available from: https://doi.org/10.1038/s43017-019-0001-x

Schiemann, R., Lüthi, D. & Schär, C. (2009) Seasonality and interannual variability of the westerley jet in the Tibetan Plateau region. *Journal of Climate*, 22(11), 2940–2957. Available from: https://doi.org/10.1175/2008JCLI2625.1

Sha, Y., Ren, X., Shi, Z., Zhou, P., Li, X. & Liu, X. (2020) Influence of the Tibetan Plateau and its northern margins on the mid-latitude Westerly Jet over Central Asia in summer. *Palaeogeography, Palaeoclimatology, Palaeoecology*, 544, 109611. Available from: https://doi.org/10.1016/j.palaeo.2020.109611

Shaw, T.E., Miles, E.S., Chen, D., Jouberton, A., Kneib, M., Fugger, S. et al. (2022) Multi-decadal monsoon characteristics and glacier response in High Mountain Asia. *Environmental Research Letters*, 17(10), 104001. Available from: https://doi.org/10.1088/1748-9326/ac9008

Slättberg, N., Lai, H., Chen, X., Ma, Y. & Chen, D. (2022) Spatial and temporal patterns of planetary boundary layer height during 1979–2018 over the Tibetan Plateau using ERA5. *International Journal of Climatology*, 42(6), 3360–3377. Available from: https://doi.org/10.1002/joc.7420

Sun, L., Yang, Y., Fu, Y., Zhang, X., Zhong, L., Zhao, C. et al. (2022) Summertime atmospheric water vapor transport between Tibetan Plateau and its surrounding regions during 1990–2019: boundary discrepancy and interannual variation. *Atmospheric Research*, 275, 106237. Available from: https://doi.org/10.1016/j.atmosres.2022.106237

Tao, S.Y., Zhang, Q.Y. & Zhang, S.L. (2001) An observational study on the behavior of the subtropical high over the West Pacific in summer. *Acta Meteorologica Sinica*, 59, 747–758. Available from: https://doi.org/10.11676/qxxb2001.078

Trenberth, K.E., Dai, A., Rasmussen, R.M. & Parsons, D.B. (2003) The changing character of precipitation. *Bulletin of the*

American Meteorological Society, 84(9), 1205–1218. Available from: https://doi.org/10.1175/BAMS-84-9-1205

UNEP. (2022) *A scientific assessment of the third pole environment*. Nairobi, Kenya: United Nations Environment Programme (UNEP). Available from: https://www.unep.org/resources/report/scientific-assessment-third-pole-environment

Wang, B., Wu, R. & Lau, K.-M. (2001) Interannual variability of the Asian summer monsoon: contrasts between the Indian and the Western North Pacific–East Asian monsoons. *Journal of Climate*, 14(20), 4073–4090. Available from: https://doi.org/10.1175/1520-0442(2001)014<4073:IVOTAS>2.0.CO;2

Wang, B., Wu, Z., Li, J., Liu, J., Chang, C., Ding, Y. & Wu, G. (2008) How to measure the strength of the east Asian summer monsoon. *Journal of Climate*, 21, 4449–4463. Available from: https://doi.org/10.1175/2008JCLI2183.1

Wang, Z., Duan, A., Yang, S. & Ullah, K. (2017) Atmospheric moisture budget and its regulation on the variability of summer precipitation over the Tibetan Plateau. *Journal of Geophysical Research: Atmospheres*, 122(2), 614–630. Available from: https://doi.org/10.1002/2016JD025515

Xu, R., Tian, F., Yang, L., Hu, H., Lu, H. & Hou, A. (2017) Ground validation of GPM IMERG and TRMM 3B42V7 rainfall products over southern Tibetan Plateau based on a high-density rain gauge network. *Journal of Geophysical Research: Atmospheres*, 122(2), 910–924. Available from: https://doi.org/10.1002/2016JD025418

Xu, X., Lu, C., Shi, X. & Gao, S. (2008) World water tower: an atmospheric perspective. *Geophysical Research Letters*, 35(20), L20815. Available from: https://doi.org/10.1029/2008GL035867

Yan, H., Huang, J., He, Y., Liu, Y., Wang, T. & Li, J. (2020) Atmospheric water vapor budget and its long-term trend over the Tibetan Plateau. *Journal of Geophysical Research: Atmospheres*, 125(23), e2020JD033297. Available from: https://doi.org/10.1029/2020JD033297

Yang, K., Ye, B., Zhou, D., Wu, B., Foken, T., Qin, J. et al. (2011) Response of hydrological cycle to recent climate changes in the Tibetan Plateau. *Climatic Change*, 109(3–4), 517–534. Available from: https://doi.org/10.1007/s10584-011-0099-4

Yang, R., Zhu, L., Wang, J., Ju, J., Ma, Q., Turner, F. et al. (2017) Spatiotemporal variations in volume of closed lakes on the Tibetan Plateau and their climatic responses from 1976 to 2013. *Climatic Change*, 140(3–4), 621–633. Available from: https://doi.org/10.1007/s10584-016-1877-9

Yao, T., Bolch, T., Chen, D., Gao, J., Immerzeel, W., Piao, S. et al. (2022) The imbalance of the Asian water tower. *Nature Reviews Earth & Environment*, 3(10), 618–632. Available from: https://doi.org/10.1038/s43017-022-00299-4

Yao, T., Xue, Y., Chen, D., Chen, F., Thompson, L., Cui, P. et al. (2019) Recent third pole's rapid warming accompanies cryospheric melt and water cycle intensification and interactions between monsoon and environment: multidisciplinary approach with observations, modeling, and analysis. *Bulletin of the American Meteorological Society*, 100(3), 423–444. Available from: https://doi.org/10.1175/BAMS-D-17-0057.1

You, Q., Kang, S., Ren, G., Fraedrich, K., Pepin, N., Yan, Y. et al. (2011) Observed changes in snow depth and number of snow days in the eastern and central Tibetan Plateau. *Climate Research*, 46(2), 171–183. Available from: https://doi.org/10.3354/cr00985

Yuan, X., Yang, K., Lu, H., He, J., Sun, J. & Wang, Y. (2021) Characterizing the features of precipitation for the Tibetan Plateau among four gridded datasets: detection accuracy and spatio-temporal variabilities. *Atmospheric Research*, 264, 105875. Available from: https://doi.org/10.1016/j.atmosres.2021.105875

Zhang, C., Tang, Q. & Chen, D. (2017) Recent changes in the moisture source of precipitation over the Tibetan Plateau. *Journal of Climate*, 30(5), 1807–1819. Available from: https://doi.org/10.1175/JCLI-D-15-0842.1

Zhang, C., Tang, Q., Chen, D., van der Ent, R.J., Liu, X., Li, W. et al. (2019a) Moisture source changes contributed to different precipitation changes over the northern and southern Tibetan Plateau. *Journal of Hydrometeorology*, 20(2), 217–229. Available from: https://doi.org/10.1175/JHM-D-18-0094.1

Zhang, H., Gao, Y., Xu, J., Xu, Y. & Jiang, Y. (2019b) Decomposition of future moisture flux changes over the Tibetan Plateau projected by global and regional climate models. *Journal of Climate*, 32(20), 7037–7053. Available from: https://doi.org/10.1175/JCLI-D-19-0200.1

Zhang, R. (2015) Changes in East Asian summer monsoon and summer rainfall over eastern China during recent decades. *Science Bulletin*, 60(13), 1222–1224. Available from: https://doi.org/10.1007/s11434-015-0824-x

Zhang, X., Chen, D. & Yao, T. (2018) Evaluation of circulation-type classifications with respect to temperature and precipitation variations in the central and eastern Tibetan Plateau. *International Journal of Climatology*, 38(13), 4938–4949. Available from: https://doi.org/10.1002/joc.5708

Zhang, Y. & Huang, D. (2011) Has the East Asian westerly jet experienced a poleward displacement in recent decades? *Advances in Atmospheric Sciences*, 28(6), 1259–1265. Available from: https://doi.org/10.1007/s00376-011-9185-9

Zhao, Y. & Zhou, T. (2021) Interannual variability of precipitation recycle ratio over the Tibetan Plateau. *Journal of Geophysical Research: Atmospheres*, 126(2), e2020JD033733. Available from: https://doi.org/10.1029/2020JD033733

Zhou, W., Leung, L.R. & Lu, J. (2022) Seasonally and regionally dependent shifts of the atmospheric westerly jets under global warming. *Journal of Climate*, 35(16), 5433–5447. Available from: https://doi.org/10.1175/JCLI-D-21-0723.1

Zhu, Y., Sang, Y.-F., Chen, D., Sivakumar, B. & Li, D. (2020) Effects of the South Asian summer monsoon anomaly on interannual variations in precipitation over the south-central Tibetan Plateau. *Environmental Research Letters*, 15(12), 124067. Available from: https://doi.org/10.1088/1748-9326/abc71b

SUPPORTING INFORMATION

Additional supporting information can be found online in the Supporting Information section at the end of this article.

How to cite this article: Lai, H.-W., Chen, D., & Chen, H. W. (2023). Precipitation variability related to atmospheric circulation patterns over the Tibetan Plateau. *International Journal of Climatology*, 1–17. https://doi.org/10.1002/joc.8317